Solar Physics
DOI: 10.1007/•••••-•••-•••-••••-•

Global-Mode Analysis of Full-Disk Data from the *Michelson Doppler Imager* and *Helioseismic and Magnetic Imager*

Timothy P. Larson[1] · **Jesper Schou**[2]

Abstract Building upon our previous work, in which we analyzed smoothed and subsampled velocity data from the *Michelson Doppler Imager* (MDI), we extend our analysis to unsmoothed, full-resolution MDI data. We also present results from the *Helioseismic and Magnetic Imager* (HMI), in both full-resolution and processed to be a proxy for the low-resolution MDI data. We find that the systematic errors we saw previously, namely peaks in both the high-latitude rotation rate and normalized residuals of odd a-coefficients, are almost entirely absent in both full-resolution analyses. Furthermore, we find that both systematic errors seem to depend almost entirely on how the input images are apodized, rather than on resolution or smoothing. Using the full-resolution HMI data, we confirm our previous findings regarding the effect of using asymmetric profiles on mode parameters, and also find that they occasionally result in more stable fits. We also confirm our previous findings regarding discrepancies between 360-day and 72-day analyses. We further investigate a six-month period previously seen in f-mode frequency shifts using the low-resolution datasets, this time accounting for solar-cycle dependence using magnetic-field data. Both HMI and MDI saw prominent six-month signals in the frequency shifts, but we were surprised to discover **that** the strongest signal at that frequency occurred in the mode coverage for the low-resolution proxy. Finally, a comparison of mode parameters from HMI and MDI shows that the frequencies and a-coefficients agree closely, encouraging the concatenation of the two datasets.

Keywords: Helioseismology, Observations; Oscillations, Solar

1. Introduction

Designed to be the successor to the *Michelson Doppler Imager* (MDI: Scherrer *et al.*, 1995) onboard the *Solar and Heliospheric Observatory* (SOHO), the *He-*

[1] Stanford University, Stanford, California, USA email: tplarson@sun.stanford.edu
[2] Max-Planck-Institut für Sonnensystemforschung, Göttingen, Germany

lioseismic and Magnetic Imager (HMI: Schou *et al.*, 2012) was launched onboard the *Solar Dynamics Observatory* (SDO) in February 2010. The designs of the two instruments are quite similar; here we shall note the differences between the two projects most pertinent to global-mode analysis. HMI is equipped with a 4096×4096 pixels CCD and takes images with a spatial resolution of approximately 0.5 arcsec per pixel, or about four times that of MDI. SDO is in geosynchronous orbit, whereas SOHO orbits the Sun–Earth L_1 Lagrange point; partially for this reason, HMI is able to send down much more telemetry. Among other observables, HMI produces full-resolution dopplergrams at a cadence of 45 seconds. Lastly, HMI observes the Fe I 6173 Å spectral line, so it sees a slightly lower height in the solar atmosphere than MDI, which observed the Ni I 6768 Å line (Fleck, Couvidat, and Straus, 2011).

Global-mode analysis of data from MDI's Medium-ℓ Program and systematic errors therein were described by Larson and Schou (2015), hereafter referred to as LS15. Before an attempt is made to extend this medium-ℓ analysis to HMI data, it is fitting to apply it to the MDI full-disk data and compare the results. Although one might expect the two MDI analyses to be in near-perfect agreement, our investigation reveals surprising differences. In particular, systematic errors such as the "bump" seen in the normalized residuals of the odd a-coefficients and the anomalous peak in the near-surface rotation rate at high latitudes have different characteristics in the analysis of full-disk data.

MDI full-disk data are available throughout the mission, but usually with a low duty cycle. Nominally, for two months per year telemetry was allocated to send down the full-disk images continuously. These time intervals constitute the Dynamics Program. As discussed in the next section, the actual lengths of the full-disk observing campaigns varied widely across the mission, as well as their timing within the year.

One might say that the primary difference between the MDI full-disk data and low-resolution data (labelled vw_V, see LS15) is that the latter are smoothed and subsampled (see Section 3), leaving them with a resolution one-fifth that of the full-disk data. However, another important difference lies in the data cropping. Whereas the vw_V data are cropped to 90 % of the average solar radius onboard the spacecraft, the full-disk data extend significantly closer to the limb. Further details are provided in Section 3.

In order to provide continuity with the MDI Medium-ℓ Program, we use the HMI data to create a vw_V proxy. This also allows us to further investigate periodicities seen in the f-mode frequencies from the analysis of MDI vw_V data.

In the next section we describe the datasets used in our analysis. In Section 3 we discuss how these data were analyzed, with emphasis on how each analysis differs from the analysis in LS15. Section 4 gives the results, first for MDI and then for HMI, followed by a comparison of the two instruments. Section 5 describes a six-month periodicity in data from both MDI and HMI and discusses the effect of B_0 (the heliographic latitude of the sub-observer point) on leakage matrices and the resulting inversions for solar rotation. Finally, in Section 6 we discuss our findings and propose how we might move forward.

2. Data

Beginning in 1996, MDI was continuously operated in full-disk mode for a few months each year through 2010. We therefore have 15 time intervals to analyze, known as the dynamics runs. To choose the exact intervals to use for global-mode analysis, one must balance the lengths of the timeseries and their duty cycles. For the most part, we have followed previous investigators, notably Rabello-Soares, Korzennik, and Schou (2008) and Rhodes *et al.* (2011). In our case, the simplest criterion is maximizing mode coverage. Another factor **that** we consider is choosing intervals similar to each other **in length** in order to facilitate comparing them.

For the year 2000 only 45 days of continuous data were available and for 2003 only 38 days were available. There were, however, small additional sections of continuous data for those years, separated from the previously used time intervals by sections with a low duty cycle. We therefore extended both timeseries. In 2002 the situation was reversed; more data were available on the other side of a large gap, but including it did not result in substantially increased mode coverage. Therefore we chose a length that was closer to the other dynamics runs.

The first part of Table 1 shows the timeseries **that** we used for the analysis presented here. The second part of the table shows timeseries used in various other investigations. In both cases processing was carried out through the mode fitting. The timeseries and resulting mode parameters can be downloaded from Stanford's Joint Science Operation Center (see the Appendix for details). The exception is the 12-day long interval in 2003, which was too short for the mode fitting to succeed, so only timeseries are available.

In order to make comparisons with the vw_V data, we use the same 15 time intervals for two other analyses. Firstly, we use the regular vw_V data. Secondly, we use the full-disk images but apodize them ~~like~~ **in the same way as** the vw_V data. We also attempted to use the full-disk apodization on vw_V images that we reconstructed from the full-disk images, but this was only possible for the years 1996 and 1998, because for the other years the gaussian convolution kernel used for the smoothing reached outside the full-disk crop radius, resulting in the loss of large amounts of data. These last two variations in the analysis required the computation of new leakage matrices. Details of the apodization are provided in the next section.

In all cases, we use a window function common[1] to all analyses for each time interval as input to the gapfilling. The result was mainly to discard a large amount of the regular vw_V data. We did not repeat the analysis of the regular full-disk data using the common window function, but the native window function included at most 0.23 % more data.

HMI began producing regular science data on 30 April 2010. Since that time, we have been performing medium-ℓ analysis of it using 72-day long timeseries in phase with the original MDI medium-ℓ timeseries. The time intervals for which

[1]The window function is a timeseries of ones and zeros designating good and bad data points respectively. The common window function is the product of two or more ~~others~~ **other corresponding window functions**.

Table 1. Dynamics timeseries. Day numbers refer to the first day of the timeseries and are given relative to the MDI epoch of 1 January 1993 00:00:00_TAI. All timeseries begin on the first minute of the start date and end on the last minute of the end date. Duty cycles are given for the raw timeseries (DC1) and the timeseries after gapfilling (DC2). The number of modes fitted with six a-coefficients (NM6) and with 36 a-coefficients (NM36) is also given. The first part of the table shows the timeseries used for this article; the second part shows timeseries used for various other investigations. ~~See the main text for details.~~

Day	Length [Days]	Start Date	End Date	DC1	DC2	NM6	NM36
1238	63	23 May 1996	24 Jul 1996	0.93	0.98	2039	1729
1563	93	13 Apr 1997	14 Jul 1997	0.91	0.98	2106	1840
1834	92	09 Jan 1998	10 Apr 1998	0.90	0.97	2132	1862
2262	77	13 Mar 1999	28 May 1999	0.92	0.97	2101	1809
2703	98	27 May 2000	01 Sep 2000	0.74	0.89	2056	1770
2980	90	28 Feb 2001	28 May 2001	0.91	0.97	2088	1837
3331	109	14 Feb 2002	02 Jun 2002	0.85	0.96	2092	1839
3904	76	10 Sep 2003	24 Nov 2003	0.58	0.75	1988	1603
4202	65	04 Jul 2004	06 Sep 2004	0.87	0.96	2062	1741
4558	67	25 Jun 2005	30 Aug 2005	0.92	0.98	2082	1755
4830	62	24 Mar 2006	24 May 2006	0.89	0.98	2073	1723
5454	58	08 Dec 2007	03 Feb 2008	0.87	0.98	2032	1687
5540	64	03 Mar 2008	05 May 2008	0.85	0.96	2088	1740
5981	65	18 May 2009	21 Jul 2009	0.75	0.84	2017	1631
6335	67	07 May 2010	12 Jul 2010	0.85	0.93	2031	1704
2703 [a]	45	27 May 2000	10 Jul 2000	0.93	1.00	1919	1556
3296 [b]	27	10 Jan 2002	05 Feb 2002	0.86	0.93	1864	1127
3331 [b]	98	14 Feb 2002	22 May 2002	0.86	0.97	2081	1821
3368 [a]	72	23 Mar 2002	02 Jun 2002	0.90	0.97	2056	1717
3904 [b]	12	10 Sep 2003	21 Sep 2003	0.81	0.98	0	0
3942 [a]	38	18 Oct 2003	24 Nov 2003	0.81	0.94	1921	1367

[a] Rabello-Soares, Korzennik, and Schou (2008)
[b] Rhodes, private communication (2017)

results are presented here are shown in Table 2. We have also created 360-day long timeseries by concatenating the gapfilled 72-day long timeseries.

3. Method

The MDI full-disk data are processed in almost exactly the same way as the vw_V data, that is, using the updated methodology described by LS15. The most notable exception is that for the full-disk data it is possible to use a larger fraction of the input images; whereas the the vw_V data are apodized with a cosine in fractional image radius from 0.83 to 0.87, the full-disk data are apodized in the same way from 0.90 to 0.95. It should also be noted that each analysis uses a leakage matrix appropriate to the data used. For the full-disk data, the leakage

Table 2. HMI timeseries. Day numbers refer to the first day of the timeseries and are given relative to the MDI epoch. Duty cycles are given for the raw timeseries (DC1) and the timeseries after gapfilling (DC2).

Day	Start Date	DC1	DC2	Day	Start Date	DC1	DC2
6328	30 Apr 2010	0.996	1.000	7408	14 Apr 2013	0.986	0.991
6400	11 Jul 2010	0.982	0.995	7480	25 Jun 2013	0.990	0.997
6472	21 Sep 2010	0.968	0.995	7552	05 Sep 2013	0.967	0.997
6544	02 Dec 2010	0.989	0.995	7624	16 Nov 2013	0.993	0.997
6616	12 Feb 2011	0.963	0.991	7696	27 Jan 2014	0.969	0.997
6688	25 Apr 2011	0.997	1.000	7768	09 Apr 2014	0.989	0.995
6760	06 Jul 2011	0.987	0.997	7840	20 Jun 2014	0.991	0.997
6832	16 Sep 2011	0.966	0.991	7912	31 Aug 2014	0.972	1.000
6904	27 Nov 2011	0.990	0.997	7984	11 Nov 2014	0.992	0.997
6976	07 Feb 2012	0.966	0.997	8056	22 Jan 2015	0.963	0.991
7048	19 Apr 2012	0.998	1.000	8128	04 Apr 2015	0.989	0.993
7120	30 Jun 2012	0.990	0.997	8200	15 Jun 2015	0.989	0.997
7192	10 Sep 2012	0.971	0.997	8272	26 Aug 2015	0.970	0.997
7264	21 Nov 2012	0.993	0.997	8344	06 Nov 2015	0.978	0.990
7336	01 Feb 2013	0.972	0.997	8416	01 Jan 2016	0.972	0.997

matrix is calculated as described by LS15, except that the input images are not convolved with anything. In particular, we have not accounted for any point spread function, but this is expected to have little effect in the medium-ℓ regime

In summary, all analysis of MDI data presented here are corrected for various geometric effects during spherical harmonic decomposition: image-scale errors, cubic distortion from the instrument optics, misalignment of the CCD, an error in the inclination of the Sun's rotation axis, and a potential tilt of the CCD. The spherical harmonic timeseries are then detrended and gapfilled as described by LS15, and Fourier transforms of these are fit to extract the mode parameters. The fitting, or peakbagging as it is called, takes into account horizontal displacement at the solar surface and the distortion of eigenfunctions by the differential rotation (known as the "Woodard effect") (Woodard, 1989). For the native full-disk analysis, the peakbagging is also repeated using asymmetric mode profiles in addition to the normally used symmetric profiles.

For the analysis of HMI data, the input images are already corrected for optical distortion. Hence, the only geometrical correction applied here is for the inclination error mentioned in the previous paragraph. After the spherical harmonic decomposition, the HMI data are processed **in** almost exactly ~~like~~ **the same way as** the MDI full-disk data. In particular, the images are apodized in the same way, and therefore an identical leakage matrix is used. The peakbagging is performed using both symmetric and asymmetric mode profiles for both the 72-day long timeseries and the 360-day long timeseries.

In addition, we have created a proxy for the MDI vw_V data from the HMI data. This is done by binning the HMI data by a factor of four to simulate the MDI full-disk data, convolving them with a gaussian, and retaining only every

fifth point in each direction as described by LS15. The resulting images are then apodized ~~like~~ **in the same way as** the MDI vw_V data, and the peakbagging likewise uses the same leakage matrix. We have fit these data only as 72-day long timeseries and only using symmetric profiles.

Whether we use the HMI images in their native resolution or by way of the proxy, the most signficant difference with the MDI processing is in the detrending. Whereas the MDI data needed to have discontinuities in the timeseries manually identified, for HMI this information can be derived from keywords in the input data. Furthermore, the quality of the HMI data are more carefully tracked, so the keywords also provide a reliable measure of what data are expected to be present.

Due to its orbit and problems with calibration, the HMI spherical harmonic timeseries contain a strong daily oscillation. We therefore detrend them using different parameters than **those used for** the MDI data. Although in both cases the timeseries are detrended by subtracting Legendre polynomials of degree seven, for HMI these polynomials are fit to an interval of 1100 points (825 minutes), which is advanced by 960 points (720 minutes). In other words, the detrending intervals overlap by 140 points (105 minutes). For additional details, the reader is referred to LS15.

4. Results

4.1. MDI Mode Parameters

In total, we applied four different analyses to all 15 **of the** dynamics runs. For conciseness, we shall make use of the following additional labels: fd_ap90 for the full-disk analysis using its regular apodization, fd_ap90_as for the same thing fit with asymmetric profiles, and fd_ap83 for the full-disk data apodized like the vw_V data. We shall use the label vw_ap83 when we use the vw_V with its regular apodization, but note that we processed it using a window function common to all analyses. We shall also use the label vw_ap90 for the vw_V data apodized like the full-disk data, but note that this analysis is only available for the 1996 and 1998 dynamics runs. Figure 1 shows the number of modes fitted using six a-coefficients (which parameterize the dependence of the frequencies on m, see LS15) for all **of** these analyses. As expected from our previous work, the mode coverage for the fd_ap90_as analysis as a function of time is basically the same as that for the fd_ap90 analysis shifted downward. Interestingly, the other two analyses are closer in coverage to the fd_ap90 analysis, with the exception of the 2003 dynamics run, which by far had the lowest duty cycle. Apparently the regular full-disk analysis was less susceptible to this low duty cycle than all **of** the other ~~ones~~ **analyses**. The effect of using asymmetric profiles on the mode parameters themselves will be discussed in the context of the HMI analysis.

In order to compare two different analyses, we must create common modesets. For example, in order to quantify the effect of the apodization, for each dynamics run we find the modes common to the fd_ap90 and fd_ap83 analyses. For each mode parameter, we then take a weighted average in time over whatever

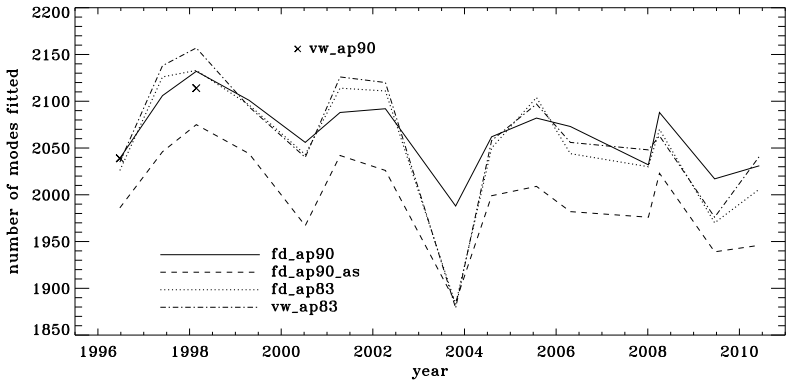

Figure 1. Mode coverage for all dynamics runs. Symbols show the number of modes fitted in 1996 and 1998 by the vw_ap90 analysis.

dynamics runs had each mode successfully fit in both analyses. For the weights, we have used the length of each timeseries ~~times~~ **multiplied by** its duty cycle. We have also computed the average error, rather than the error on the average, and for comparison between two analyses we use the larger error estimate of the two. Thus the significance **that** we show is the least **that** one might expect from an average dynamics run. Lastly, the noise parameter $[b]$ requires special treatment. Since e^b is proportional to the length of the timeseries, each background parameter has $\log(T/72.0)$ subtracted from it before averaging, where T is the length of the timeseries in days. Except where noted, we have used the ~~parameters fit~~ **fitted parameters resulting from** using six a-coefficients.

In Figure 2 we show the result for six mode parameters: frequency, amplitude, width, background, a_1, and a_2. For a full explanation of these, the reader is referred to LS15. Clearly, the most significant change is to the amplitudes. One might think **that** this is to be expected since the fd_ap83 data are apodized to a smaller radius, but in fact this ought to be corrected for in the leakage matrix. In other words, the parameter A should represent the intrinsic amplitude of the mode *on the Sun*. Next most significant is the change to the background, which was lower for the fd_ap83 analysis at lower frequencies, and higher at higher frequencies. The widths were lower for the fd_ap83 analysis across all frequencies, especially between 2.0 and 3.0 mHz. Lastly, although not very significant, the bump seen in the difference in a_1 is encouraging, since it is in the same location as the bump **that** we hope to eliminate.

Here we note that in the absense of systematic errors, these differences should all be small ($\ll 1\sigma$) near the peak power of the p-mode band (around 3.0 mHz), since the signal-to-noise ratio is high there (Libbrecht, 1992). In any case, the differences should have no trends in frequency or any other parameter. One source of random error, the stochastic excitation of the modes, is the same for all observers and apodizations, since ~~over the majority of the medium-ℓ range the modes~~ **the modes considered here** have long enough lifetimes to be considered truly global. Another source of random error, convective motions on the surface,

could be different when using different parts of the solar disk, but this still should not cause any offsets in the frequencies, widths, or a-coefficients. Although the amplitudes and background parameters could be affected, such an effect would still be flat in frequency. Even when the signal-to-noise ratio is low, the changes should still be random. Hence, we can already see that there is a problem with the analysis.

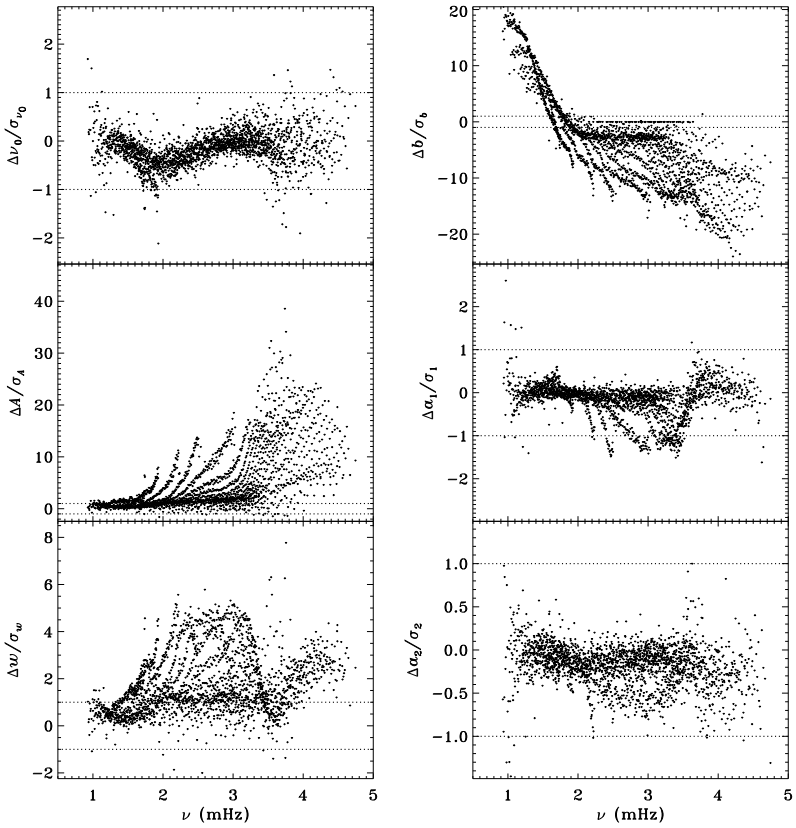

Figure 2. Effect of apodization on mode parameters. Shown are changes in frequency [ν_0], amplitude [A], width [w], background parameter [b], a_1, and a_2 in units of **the** standard deviation. Each panel is scaled differently; ~~dotted~~ **horizontal** lines show the $\pm1\sigma$ levels. For the a-coefficients, no more than nine points have been excluded from the range shown. The sense of subtraction is fd_ap90 minus fd_ap83.

To quantify the effect of smoothing and subsampling, we compare the fd_ap83 and vw_ap83 analyses in exactly the same fashion. Figure 3 shows the results. Here the convective noise is the same, as well as any instrumental effect, since the two datasets observe almost the same part of the solar disk. Indeed, with the exception of the background parameter, the smoothing and subsampling results in smaller changes than the apodization. The average of the other parameters shows almost no significance at all. In particular, the differences in the a-coefficients are hardly different from zero, which would suggest that the smoothing and subsampling has little effect on any inversion results.

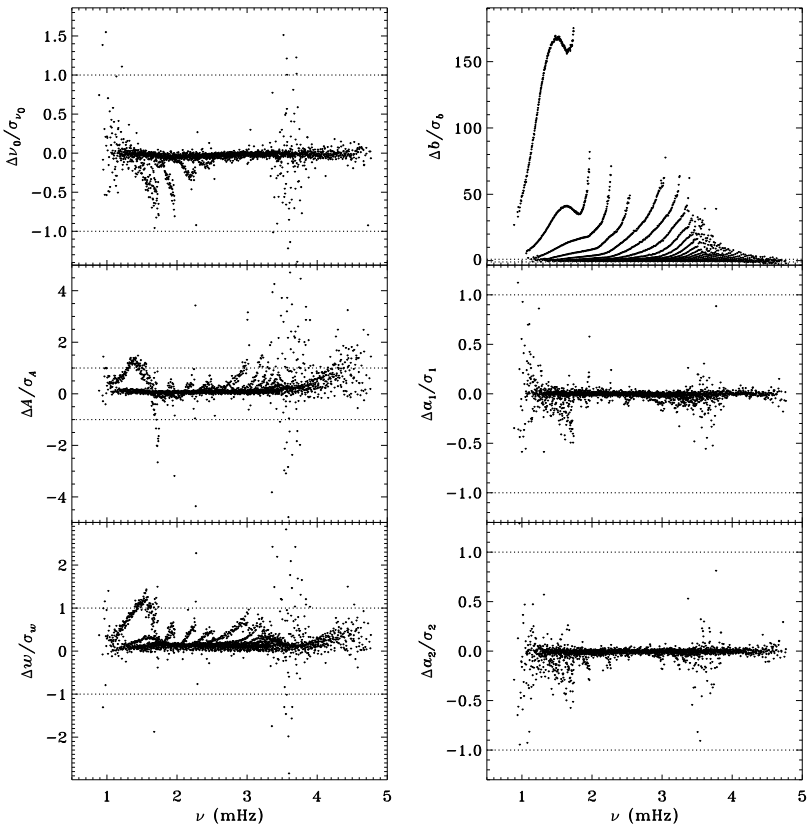

Figure 3. Effect of smoothing and subsampling on mode parameters. Shown are changes in frequency [ν_0], amplitude [A], width [w], background parameter [b], a_1, and a_2 in units of **the** standard deviation. For clarity, the bottom panels have at most 0.65 % of points excluded. Each panel is scaled differently; ~~dotted~~ **horizontal** lines show the $\pm 1\sigma$ levels. The sense of subtraction is fd_ap83 minus vw_ap83.

The small difference for the amplitude shown in Figure 3 is, however, deceptive. For all other parameters, the differences look roughly the same for the different dynamics runs, but for the amplitudes, the difference actually alternates in sign. This is shown in Figure 4, where we have plotted the mean signficance as a function of time. We have as yet no explanation for this oscillation, but focus and tuning changes in the instrument are likely candidates.

4.2. Systematic Errors in MDI data

To explore the effect of the different analyses on our systematic errors, we begin by performing simple one-dimensional regularized least-squares (RLS) rotational inversions using the a_1-coefficient only, just as in LS15. In this case, we formed modesets common to all three of the fd_ap90, fd_ap83, and vw_ap83 analyses for each dynamics run, and **we** took the **temporal** average ~~in time~~ as before, except that for inversions we always use the error on the average. The tradeoff

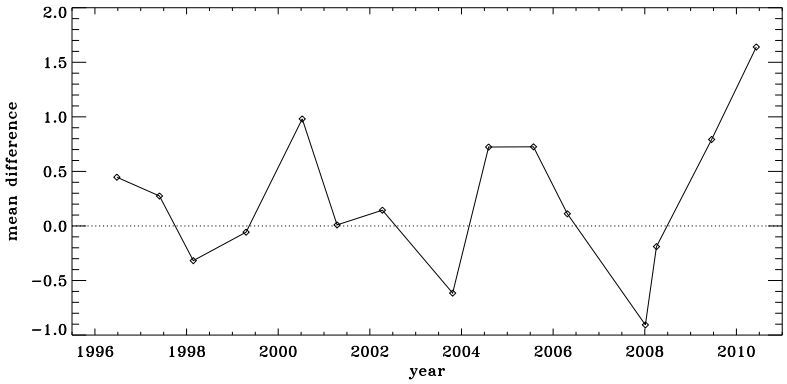

Figure 4. Effect of smoothing and subsampling on amplitudes. Shown are the mean changes in units of **the** standard deviation, for all dynamics runs. The sense of subtraction is fd_ap83 minus vw_ap83.

curves in Figure 5 show the result. The curve for the fd_ap90 analysis has the shape one hopes to see: a single "elbow" so that one may unambiguously choose a tradeoff parameter, not to mention that the χ^2 values are closer to unity. It is satisfying to see that the value typically used, $\mu = 10^{-6}$, lies right where it should on the curve: "the place where the residuals stop decreasing sharply, so that further decreases of μ will be of little benefit" (LS15). The other two curves are very close to the final curve we found in LS15, and we have marked the tradeoff parameters **that** we used previously.

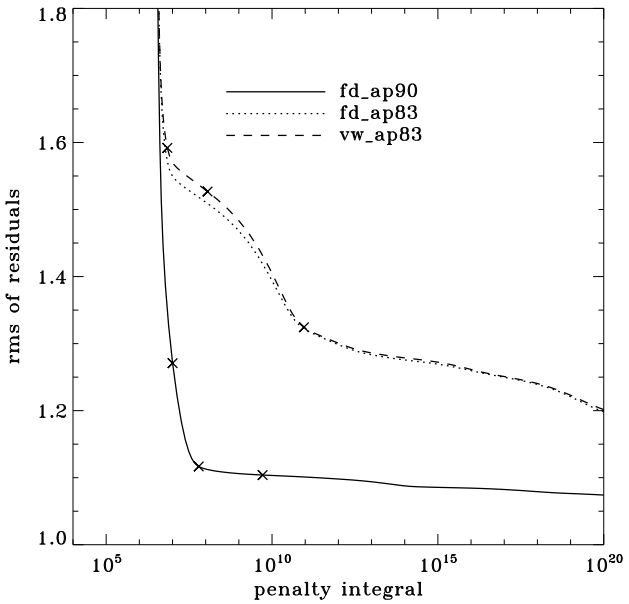

Figure 5. Tradeoff curves for an average over all dynamics runs. Symbols, from left to right, indicate tradeoff parameters of $\mu = 10^{-4}$, $\mu = 10^{-6}$, and $\mu = 10^{-9}$.

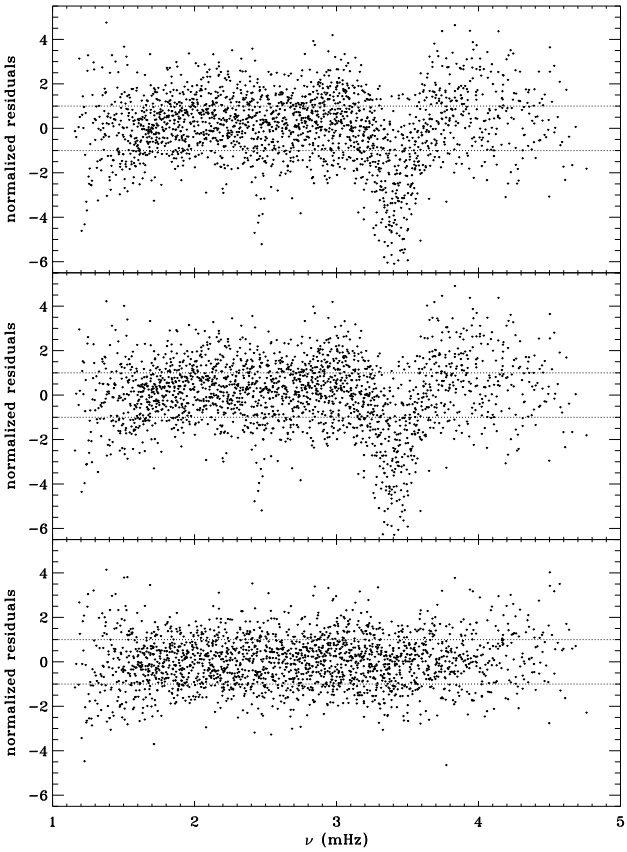

Figure 6. Normalized residuals of a_1 for an average over all dynamics runs. Shown from top to bottom are the vw_ap83 analysis, the fd_ap83 analysis, and the fd_ap90 analysis. ~~Dotted~~ **Horizontal** lines show the $\pm 1\sigma$ levels.

In order to see how the different analyses affect our inference of how the solar rotation varies with latitude, we perform two-dimensional RLS inversions using 36 a-coefficients. First, we form averages over the dynamics runs just as we did for the one-dimensional inversions. The residuals of a_1 resulting from inversions of these averages are shown in Figure 6. As one can see, the analyses using the vw_V apodization clearly show the bump, whereas it is essentially absent from the fd_ap90 analysis. Investigating the polar jet **(LS15)**, we found that it was clearly visible in inversions of the 1998 dynamics run alone, so we are able to compare all four analyses. Again, we took the modeset common to all four. As Figure 7 shows, we again see that using a smaller apodization radius results in the polar jet, while the larger apodization radius shows no sign of it. Here we must reiterate that the bump does not cause the jet; previous research has shown that excluding from the inversion modes that constitute the bump still shows the jet (Schou *et al.*, 2002). Hence, for both the bump and the jet, we are left with a puzzle. Using the vw_V apodization results in both of the systematic errors, which are then removed by using *more* data from the input images, although the

data added ~~is~~ **are** expected to contain only a small fraction of the helioseismic signal. The most likely explanation is an error in the analysis codes or leakage matrix, but so far no error explaining our results has ~~not~~ been found.

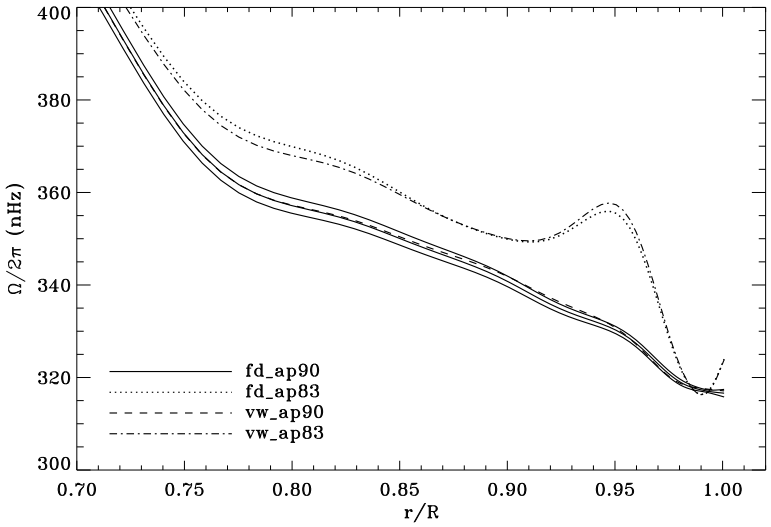

Figure 7. Internal rotation as a function of radius at 75° latitude for four analyses applied to the 1998 dynamics run. Solid lines show the fd_ap90 analysis and its error; errors for the other analyses were similar.

4.3. HMI Mode Parameters

We have so far analyzed about six years of HMI data, as both 72-day and 360-day fits for the full-disk data, using both symmetric and asymmetric profiles. For the vw_V proxy, we have used only 72-day long timeseries and symmetric profiles. The resulting number of modes fitted is shown in Figure 8. The difference in coverage between symmetric and asymmetric fits and between 360-day fits and 72-day fits is what we have come to expect based on our analysis of other datasets. Surprising, however, is the large oscillation in coverage of the fits to the vw_V proxy data, especially since it exceeds the coverage of the full-disk fits at its peak. We shall return to this fact later.

In LS15 we found that the fits using asymmetric profiles are much less stable than those using symmetric profiles. This is not surprising, since the asymmetric fits require an extra parameter, but it does result in decreased mode coverage. However, in the region where the modes are observed to have strong asymmetry, one must accept that using asymmetric profiles more accurately characterizes them. Hence, the parameters resulting from both types of fitting have become standard data products. The difference in coverage for the 72-day fits is shown in Figure 9, where diamonds indicate a mode that failed at least once using symmetric profiles when asymmetric profiles succeeded, and

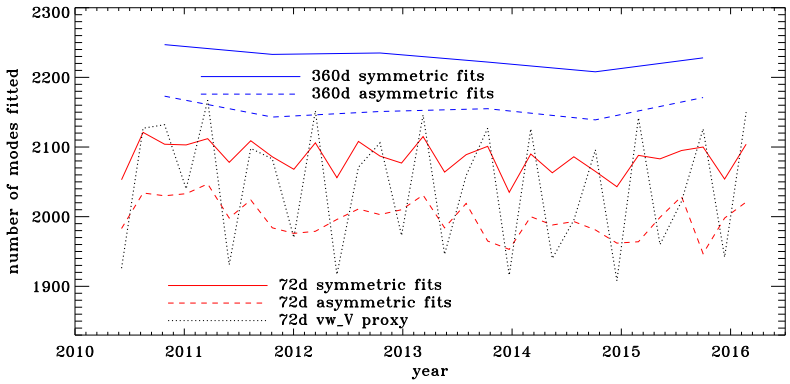

Figure 8. Number of modes fitted as a function of time for the first six years of HMI.

dots indicate a mode that failed at least once using asymmetric profiles when symmetric profiles succeeded. The difference in mode parameters themselves

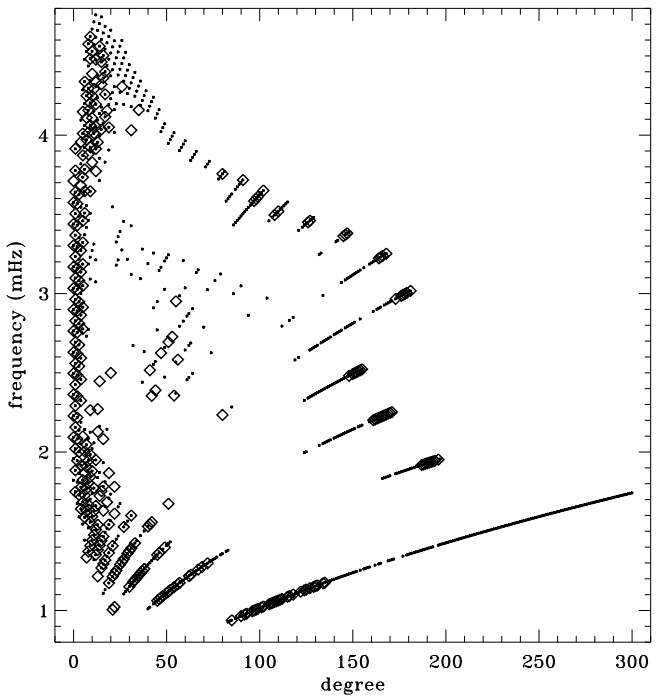

Figure 9. Difference in mode coverage for the first six years of HMI. Diamonds show modes that failed to fit at least once with symmetric profiles when asymmetric profiles succeeded, and dots show the opposite.

are shown in Figure 10, where we have performed averaging in the same manner as before, using the 72-day fits. This figure is to be compared to the last panel of Figures 4 – 8 in LS15. Clearly, fitting asymmetric profiles has a large effect on the resulting frequencies in a range between 1.0 and 3.0 mHz. The other mode

parameters were similarly, but less significantly, affected in a slightly smaller frequency range, still centered at about 2.0 mHz. For the amplitudes, widths, and background parameters, there was also a large and opposite change above 3.8 mHz, while the frequency differences show a second peak around the same frequency. Although not shown here, we found similar differences using the MDI full-disk data. Hence, we can rest assured that the asymmetry of the modes is characterized **in** the same **way** by all **of** the datasets **that** we have studied.

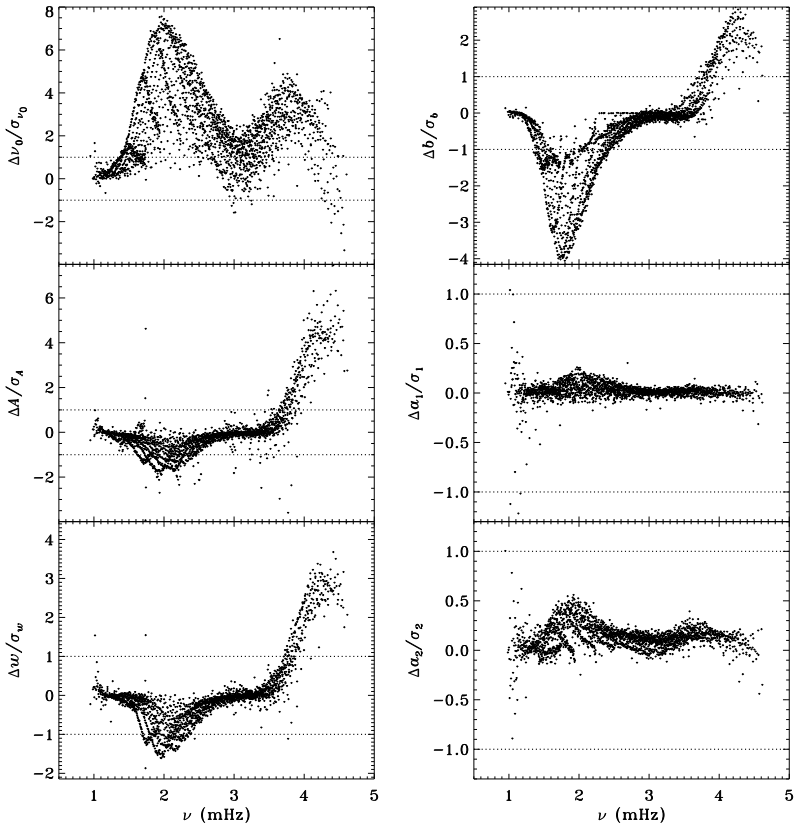

Figure 10. Effect of asymmetric profiles on mode parameters from 72-day fits. Shown are changes in frequency [ν_0], amplitude [A], width [w], background [b], a_1, and a_2 in units of **the** standard deviation. The data have been averaged over six years of HMI. Each panel is scaled differently; ~~dotted~~ **horizontal** lines show the $\pm1\sigma$ levels. At most 0.18 % of points have been excluded. The sense of subtraction is asymmetric minus symmetric.

Unfortunately, this also means that the error magnification **that** we saw for the frequencies and background parameters in LS15 is also present in the analysis of the full-disk datasets.

Our previous work also revealed discrepancies between 360-day fits and an average over 72-day fits for the MDI vw_V data, regardless of whether symmetric or asymmetric profiles were used. To confirm that this reflects a characteristic of the algorithm and not the data, we repeated the comparison for the first six years of HMI. Figure 11 shows the results using asymmetric profiles. Comparison

with Figure 13 of LS15 reveals the same trends. The exception is the amplitude differences, but this can be attributed to the gaussian smoothing applied to the vw_V data. Although not shown here, we also found error ratios similar to those shown in LS15. This would indicate that the difference has to do with the algorithm and not the data. However, Barekat, Schou, and Gizon (2014) found significant differences between the two instruments in the radial gradient of the rotation rate at high latitudes near the surface. In subsequent investigations, Barekat (private communication, 2015) also found that the results using the 360-day fits for HMI differed significantly from those using the averaged 72-day fits, while for MDI the two are essentially in agreement. Clearly, further study is needed to determine the source of these differences.

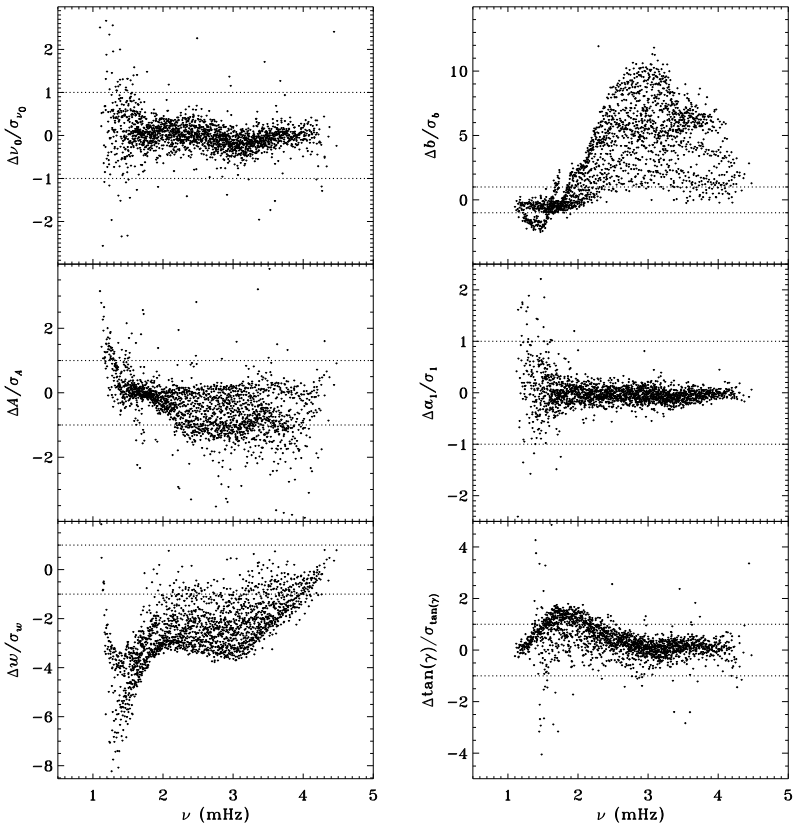

Figure 11. Difference between 360-day and 72-day fits in frequency [ν_0], amplitude [A], width [w], background [b], a_1, and tangent of the asymmetry parameter [γ] in units of **the** standard deviation. The data have been averaged over six years of HMI. Each panel is scaled differently; ~~dotted~~ **horizontal** lines show the $\pm1\sigma$ levels. At most 0.66 % of points have been excluded. The sense of subtraction is 360-day long fits minus 72-day long fits.

4.4. Systematic Errors in HMI data

We plot tradeoff curves and normalized residuals of a_1 for both the HMI full-disk and vw_V proxy analyses, shown in Figures 12 and 13, just as we did for the MDI data. Comparison reveals similar differences between the full-disk and low-resolution results as for MDI. The tradeoff curve shows higher residuals, and the bump in the residuals of a_1 is much more significant. For the rotation rate at high latitudes, HMI's ~~time~~ **temporal** coverage allowed us to discover that the jet is only discernible when $|B_0|$ is maximal, although the two analyses still resulted in significantly different rotation rates. Further, the upturn in the rotation rate near the surface at 75° is more pronounced at these times for the vw_V proxy. When B_0 is close to zero we see the upturn in both analyses, but it is stronger for the vw_V proxy. Both features are clearly seen in an average over the six years **that** we have analyzed, shown in Figure 14.

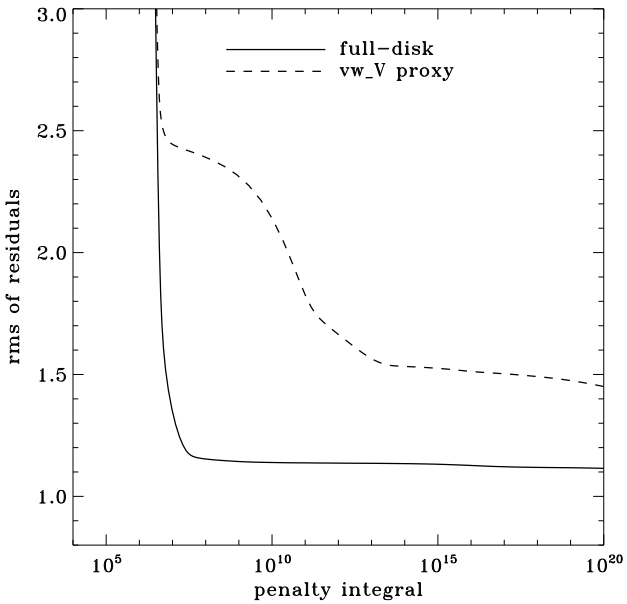

Figure 12. Tradeoff curves for an average over six years of HMI.

4.5. Comparison of MDI and HMI

Both MDI and HMI were operating during the 2010 dynamics run. Hence, we have the opportunity to compare the mode parameters resulting from each dataset. Unfortunately, since the two instruments operate at two different cadences, it is not straightforward to generate a common window function. Setting this aside, Figure 15 shows a comparison of the modes common to the fd_ap90 and regular HMI analyses for this time interval using their native window functions. Similarly, Figure 16 compares the analysis of the HMI vw_V proxy and the MDI vw_V datasets for the first 72 days of HMI. Again, since realization

noise is identical for the two instruments, we hope to to see small differences for the frequencies, widths, and a-coefficients, since these parameters should not depend on the height of formation of the respective absorption lines used for the observations.

These figures are encouraging in that the frequencies and a-coefficients do show little change between the two instruments, although there is a hint of a feature in the frequency differences around 1.7 mHz. One is not surprised to see large differences in ~~amplitude and~~ **the** background parameter, since ~~these parameters do~~ **it does** depend on the height at which the mode is observed. ~~Although the amplitude differences have different shapes in Figures 15 and 16, HMI always observed larger amplitudes for almost all modes. Unfortunately, HMI observed lower widths at low frequencies.~~ **Similarly, the fact that the amplitude differences are not the same in Figures 15 and 16 may be explained by the different center-to-limb dependence of the observing height for the two instruments. Unfortunately the widths observed by the two instruments are not consistent, with HMI systematically measuring lower values.**

To see how much of the discrepancy results from differences in the instruments and how much results from differences in the processing, Figure 17 plots the difference between the HMI full-disk fits and the fits to the vw_V proxy data for the first 72 days of HMI, while Figure 18 plots the difference between the fd_ap90 and vw_ap83 for the 2010 dynamics run. In other words, Figure 18 can be thought of as the sum of Figures 2 and 3 for a single dynamics run. The close similarity of Figures 17 and 18 gives us confidence that the observed differences have little to do with the source of the data.

5. Effect of B_0

5.1. Six-Month Periodicity

The original analysis of the vw_V data revealed a one-year period in the fractional frequency change of the f-modes. In LS15 we found that the amplitude of the annual component increased with increasing degree, but it was decreased by correcting for the Doppler shift caused by the motion of SOHO relative to the Sun. In Figure 19 we show the fractional change in f-mode frequency for the entire MDI mission using the most recent **fitted** mode parameters ~~fit~~ **resulting from** using symmetric profiles and 36 a-coefficients. The values shown have been averaged over a range in ℓ from 251 to 300 and corrected for Doppler shift. To see how the frequency shifts vary with the solar cycle, we plotted them against the average rms value of the line-of-sight magnetic field, as given by the DATARMS keyword in the corresponding data series[2]. We found a linear relation-

[2]For MDI this dataseries is mdi.fd_M_96m_lev182, which, as the name implies, samples the magnetic field at a cadence of 96 minutes. We looked at all available records for each 72-day interval and rejected outliers above 100 Gauss. The average was taken over the remaining records. For HMI, the dataseries is hmi.M_720s, which has a cadence of 12 minutes. We therefore took every eighth record to give a sampling similar to that of MDI, ~~but~~ **and** no outlier rejection was needed.

ship between the two and subtracted it. Now, rather than a one-year period, we predominantly see a six-month period, presumably related to the absolute value of B_0. To demonstrate that this is so, we overplot the two quantities in Figure 20. The correlation coefficient between the frequency shifts and the average absolute value of B_0 is 0.42.

To see if the same is true for HMI, we first apply the same procedure to the vw_V proxy, although in this case the motion of the spacecraft relative to the Sun has already been corrected for in the dopplergrams by shifting their target times. To see how the smoothing, subsampling, and apodization might affect the frequency shifts, we did the same with the HMI full-disk data. The result is shown in Figure 21, where we see that the two analyses almost always agree within their errors. In each case we then subtracted a linear function of the average magnetic field, as before. For the vw_V proxy we again see a prominent six-month signal, but it is slightly weaker than for MDI, as Figure 22 shows. In this case the correlation coefficient was 0.39. For the full-disk data the correlation was only 0.28. However, inspection of the number of modes fitted as a function of time for the vw_V proxy, shown in Figure 8, reveals exactly this period. Overplotting the absolute value of B_0 further reveals that, contrary to all expectation, mode coverage is lowest when B_0 is minimal, as Figure 23 shows. Here the correlation coefficient is 0.95. For completeness, we note that the correlation when using the full-disk data is only 0.78. Recalling that the leakage matrix is computed assuming $B_0 = 0$, it can only come as a shock that we fit more modes when the leakage matrix is most incorrect. Until this discovery one might have thought that the variation of mode parameters with B_0 was related to the approximation that the leaks from $\Delta\ell+\Delta m$ odd are zero, since it assumes north–south symmetry. It now seems much more likely that the variation has to do with what part of the solar surface is visible.

5.2. Leaks for Maximal $|B_0|$

A variation in the analysis suggested by the results of the previous section is to use a leakage matrix for a non-zero B_0. By good fortune, B_0 was near its minimum in the middle of the 1998 dynamics run, its average value being $-6.35°$. We repeated the peakbagging for this interval using full-disk leakage matrices computed for that value of B_0 for both apodizations. We must point out, however, that the results using the new leakage matrices are not necessarily any more correct than the original results, since in both cases the leaks from $\Delta\ell + \Delta m$ odd are ignored. Put another way, the leakage-matrix elements **that** we use become more accurate, but the ones **that** we ignore become different from zero. To illustrate the relative magnitude of the odd leaks, in Figure 24 we plot sensitivies to the target mode ($\Delta\ell = \Delta m = 0$) in the two cases. In Figure 25, we plot odd elements of the new leakage matrices. For the sake of brevity, we have shown only the real part of the radial component of the leakage matrix.

Athough **this is** not shown, we found that the mode parameters changed similarly for the two apodizations. The unsurprising exception was that the change in a_1 showed the bump, with marginal significance, when using the vw_V apodization. The amplitudes and background parameters showed highly

significant changes, while the changes in width were moderately significant. The results of two-dimensional RLS inversions are shown in Figure 26. Clearly a large change resulted between $0.83R_\odot$ and $0.95R_\odot$ when using the vw_V apodization, whereas the change when using the full-disk apodization was not significant. Although **this is** not shown, we also found similar results using the smoothed data. Plotting the tradeoff curves, shown in Figure 27, we see that the new leakage matrix resulted in lower residuals for both **of the** apodizations.

6. Discussion and Future Prospects

In comparing the MDI full-disk data with the vw_V data we found that the difference in mode parameters, with the exception of the background, mostly resulted from the different apodizations used in the two analyses. In particular, the difference in a_1 showed the bump at 3.4 mHz. Correspondingly, two-dimensional RLS inversions of data using the full-disk apodization did not show the bump in the residuals, whereas it appeared almost the same in the two analyses using the vw_V apodization. Likewise, the high-latitude jet was almost completely absent when using the full-disk apodization. In one-dimensional inversions, the tradeoff curve for the full-disk analysis using the vw_V apodization still showed the anomalous shape seen in LS15.

To further explore the possible cause of these discrepancies, we plotted the ratio of the amplitudes from the full-disk analysis using its regular apodization to the amplitudes found using the vw_V apodization, and likewise for the widths. The result is shown in Figure 28. The shape of these ratios is roughly the same as the differences shown in the second and third panels of Figure 2, which were plotted in units of significance. The difference in amplitudes would suggest a problem with the leakage matrix, which could also affect the widths, but those differences might also be attributed to the model **that** we use for the background. Although not shown, we found that the background differences themselves also showed a trend similar to that seen in the significance.

Smoothing and subsampling made highly significant changes only to the background parameter. Recalling that e^b multiplies the covariance of the noise at high frequencies (LS15), one might guess that the gaussian convolution somehow changes the noise in in that range. The smoothing and subsampling also made significant changes to the amplitude, and these changes varied in sign across the dynamics runs. One probable cause for the sign change is the difference between the best focus and commanded focus in the instrument, which varied throughout the mission. ~~Tuning changes are also likely to play a part.~~ **The occasional changes in the instrument tuning to compensate for drifts are also likely to play a part.** The question of how the smoothing and subsampling change the amplitude at all remains unanswered, as their effect should be accounted for in the leakage matrix. In the future, one might perform the smoothing without subsampling, since subsampled data should result in greater interpolation errors when the images are remapped, which could account for some of the differences. Other methods of smoothing and subsampling are possible, as well as measuring the covariance of the noise in different frequency intervals.

The analysis of HMI data confirmed that using a proxy for the vw_V data resulted in both the high-latitude jet and the bump in the odd a-coefficients, whereas both were essentially absent from the analysis of full-disk data. Comparison of fits using asymmetric mode profiles to those using symmetric profiles revealed differences **similar to those** ~~as~~ seen in LS15 and in the analysis of MDI full-disk data. In spite of fitting fewer modes, asymmetric profiles (occasionally) resulted in more stable fits at the ends of ridges, mostly at the low-ℓ ends, but also at the high-ℓ ends for p-modes of low to moderate radial order. Comparison of 360-day fits to an average of 72-day fits also revealed differences similar to those seen in LS15. Other investigators (Barekat, Schou, and Gizon, 2016), however, have found differences in the inversions of modesets from the two instruments, which we have not discussed here, but **which** should be investigated in the future.

HMI also allows us to compare the difference between the full-disk results and those for the vw_V proxy in the magnitude of the six-month oscillation. Although we have not examined the frequency shifts for the full-disk data, we did find the surprising result that more modes were fitted for the vw_V proxy when the absolute value of B_0 was at its peak. This might suggest that the systematic errors we see are related to the alignment of the apodization circles with the spherical harmonic node lines. To see if this is true, one might try using differently shaped apodizations, such as apodizing in longitude and latitude rather than image radius, or an elliptical apodization.

In the comparison of mode parameters from HMI and MDI, we found that differences in frequencies and a-coefficients were not significant for the full-disk analyses, and even less so for the vw_V analyses. While the frequency differences indicated a small feature, the differences in a-coefficients were almost completely flat. Since these are the only parameters used in rotational inversions, there should be no problem with concatenating datasets from the two instruments in order to increase the interval over which consistent physical inferences can be drawn. As an example, Figures 29 and 30 show internal rotation derived from full-disk datasets for MDI and HMI, respectively. Following Schou *et al.* (1998), we have removed the region where estimates of rotation are deemed unreliable. As expected, the two inferences agree quite well.

Furthermore, if we believe that the full-disk analyses are more accurate than the vw_V analyses, we can use the former to correct the latter. This is essential for MDI, since the vw_V data are the only helioseismic dataset it provided with a high duty cycle.

Acknowledgments This work was supported by NASA Contract NAS5-02139. SOHO is a mission of international cooperation between NASA and ESA. SDO is part of NASA's Living With a Star program. HMI data are provided courtesy of NASA/SDO and the HMI science team. The authors thank the *Solar Oscillations Investigation* team at Stanford University and its successor, the Joint Science Operations Center. Much of the work presented here was done while J. Schou was employed at Stanford University. T.P. Larson thanks Laurent Gizon and the Max-Planck-Institut für Sonnensystemforschung for generously hosting him during the initial composition of this article. The German Data Center for SDO is supported by the German Aerospace Center (DLR) and the State of Niedersachsen.

Disclosure of Potential Conflicts of Interest The authors declare that they have no conflicts of interest.

Appendix

Detailed information on how to access MDI data from the global helioseismology pipeline can be found on the website of the Joint Science Operations Center (JSOC) at jsoc.stanford.edu/MDI/MDI_Global.html and likewise for HMI at jsoc.stanford.edu/HMI/Global_products.html . These pages contain documentation describing how the datasets used in this ~~paper~~ **article** were made and how they can be remade. A description of these data and their keywords was also given in the Appendix of LS15; data formats and keyword names remain unchanged in this work. All mode parameters presented here, as well as the rotational inversions shown in Figures 29 and 30, are available in the electronic supplementary material. The data series from which the relevant data may be downloaded are described below.

Mode parameters resulting from both symmetric and asymmetric fits to regular full-disk data from MDI can be found in two data series: mdi.fd_V_sht_modes and mdi.fd_V_sht_modes_asym. Mode parameters for the nonstandard analyses can be found in su_tplarson.mdi_V_sht_modes. In all cases, the first primekey [(T_START)] should be specified as an MDI day number, found in Table 1, suffixed by "d". Since some of the timeseries have the same start times, in general one must also specify NDT, the number of points in the timeseries (see Table 1; an MDI timeseries has 1440 points per day). For the nonstandard analyses, the TAG keyword should also be specified; it can take values of fdvwap, vwcomm, and vwfdap corresponding to the labels fd_ap83, vw_ap83, and vw_ap90 used in this article.

For HMI, all mode parameters presented here reside in the official HMI name space (hmi). The data series are hmi.V_sht_modes and hmi.V_sht_modes_asym for the full-disk data, and the day numbers are found in Table 2. For the former data series, there is also a record corresponding to the last dynamics run. Since these series also contain both 72-day and 360-day fits, the primekey NDT should also be specified; note that an HMI timeseries has 1920 points per day. For the vw_V proxy, the data series is hmi.vw_V_sht_modes.

Newly available online are data series containing the results of two-dimensional RLS inversions for rotation. These series have the same primekeys as those containing the mode parameters and three more in addition: NACOEFF, RADEXP, and LATEXP. NACOEFF is the number of a-coefficients used in fitting the mode parameters, RADEXP is the exponent of the radial tradeoff parameter (=10^RADEXP), and LATEXP is likewise the exponent of the latitudinal tradeoff parameter. To date, only values of RADEXP=-6 and LATEXP=-2 have been used, and these are also the default values for these keywords. NACOEFF can take values of 6, 18, or the default of 36. The data available include the rotation profile, its errors, and the output a-coefficients. The data series names are the same as those given for mode parameters above, with the string modes replaced by 2drls. For a full explanation of the format of these data the reader is referred to the electronic supplementary material or the above websites. Note that at this time all online inversions have used full modesets.

For the mode parameters and inversions in the MDI and HMI namespaces used in this article, the VERSION keyword is set to version2. Furthermore, all

of the intermediate data products are also available (archived), and the data series names can be found on the above websites. For the nonstandard analyses, the gapfilled timeseries and window functions are archived; the data series are su_tplarson.mdi_XXX_V_sht_gf and su_tplarson.mdi_XXX_V_sht_gf_gaps, where XXX can be one of fdvwap, vwcomm, and vwfdap as above. The raw timeseries and window functions have not been archived, but can be recreated if needed.

References

Barekat, A., Schou, J., Gizon, L.: 2014, The radial gradient of the near-surface shear layer of the Sun. *Astron. Astrophys.* **570**, L12. DOI. ADS.

Barekat, A., Schou, J., Gizon, L.: 2016, Solar-cycle variation of the rotational shear near the solar surface. *Astron. Astrophys.* **595**, A8. DOI. ADS.

Fleck, B., Couvidat, S., Straus, T.: 2011, On the Formation Height of the SDO/HMI Fe 6173 Å Doppler Signal. *Solar Phys.* **271**, 27. DOI. ADS.

Larson, T.P., Schou, J.: 2015, Improved Helioseismic Analysis of Medium-ℓ Data from the Michelson Doppler Imager. *Solar Phys.* **290**, 3221. DOI. ADS.

Libbrecht, K.G.: 1992, On the ultimate accuracy of solar oscillation frequency measurements. *Astrophys. J.* **387**, 712. DOI. ADS.

Rabello-Soares, M.C., Korzennik, S.G., Schou, J.: 2008, Analysis of MDI High-Degree Mode Frequencies and their Rotational Splittings. *Solar Phys.* **251**, 197. DOI. ADS.

Rhodes, E.J., Reiter, J., Schou, J., Larson, T., Scherrer, P., Brooks, J., McFaddin, P., Miller, B., Rodriguez, J., Yoo, J.: 2011, Temporal changes in the frequencies of the solar p-mode oscillations during solar cycle 23. In: Prasad Choudhary, D., Strassmeier, K.G. (eds.) *Physics of Sun and Star Spots*, *IAU Symp.* **273**, Cambridge University Press, Cambridge, UK, 389. DOI. ADS.

Scherrer, P.H., Bogart, R.S., Bush, R.I., Hoeksema, J.T., Kosovichev, A.G., Schou, J., Rosenberg, W., Springer, L., Tarbell, T.D., Title, A., Wolfson, C.J., Zayer, I., MDI Engineering Team: 1995, The Solar Oscillations Investigation - Michelson Doppler Imager. *Solar Phys.* **162**, 129. DOI. ADS.

Schou, J., Antia, H.M., Basu, S., Bogart, R.S., Bush, R.I., Chitre, S.M., Christensen-Dalsgaard, J., Di Mauro, M.P., Dziembowski, W.A., Eff-Darwich, A., Gough, D.O., Haber, D.A., Hoeksema, J.T., Howe, R., Korzennik, S.G., Kosovichev, A.G., Larsen, R.M., Pijpers, F.P., Scherrer, P.H., Sekii, T., Tarbell, T.D., Title, A.M., Thompson, M.J., Toomre, J.: 1998, Helioseismic Studies of Differential Rotation in the Solar Envelope by the Solar Oscillations Investigation Using the Michelson Doppler Imager. *Astrophys. J.* **505**, 390. DOI. ADS.

Schou, J., Howe, R., Basu, S., Christensen-Dalsgaard, J., Corbard, T., Hill, F., Komm, R., Larsen, R.M., Rabello-Soares, M.C., Thompson, M.J.: 2002, A Comparison of Solar p-Mode Parameters from the Michelson Doppler Imager and the Global Oscillation Network Group: Splitting Coefficients and Rotation Inversions. *Astrophys. J.* **567**, 1234. DOI. ADS.

Schou, J., Scherrer, P.H., Bush, R.I., Wachter, R., Couvidat, S., Rabello-Soares, M.C., Bogart, R.S., Hoeksema, J.T., Liu, Y., Duvall, T.L., Akin, D.J., Allard, B.A., Miles, J.W., Rairden, R., Shine, R.A., Tarbell, T.D., Title, A.M., Wolfson, C.J., Elmore, D.F., Norton, A.A., Tomczyk, S.: 2012, Design and Ground Calibration of the Helioseismic and Magnetic Imager (HMI) Instrument on the Solar Dynamics Observatory (SDO). *Solar Phys.* **275**, 229. DOI. ADS.

Woodard, M.F.: 1989, Distortion of high-degree solar p-mode eigenfunctions by latitudinal differential rotation. *Astrophys. J.* **347**, 1176. DOI. ADS.

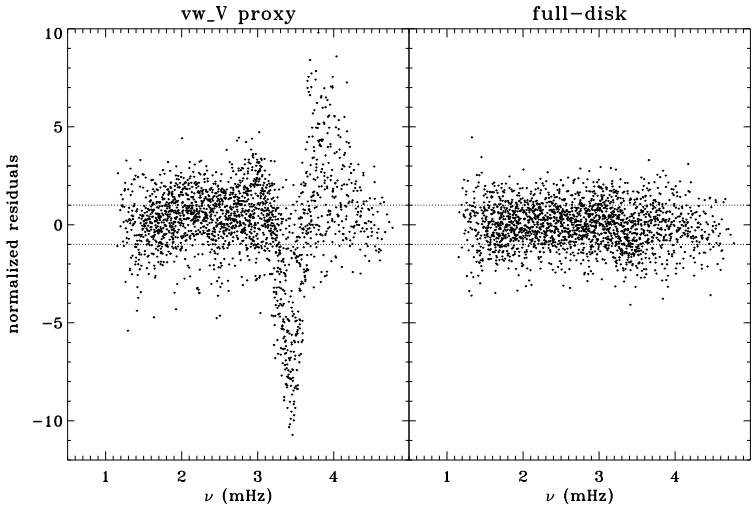

Figure 13. Normalized residuals of a_1 for an average over six years of HMI. Left panel shows the HMI vw_V proxy. Right panel shows the full-disk HMI analysis. ~~Dotted~~ **Horizontal** lines show the $\pm 1\sigma$ levels.

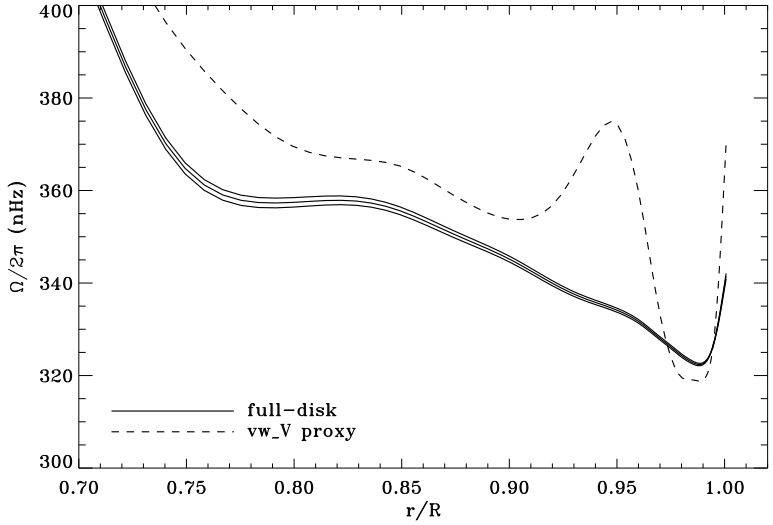

Figure 14. Internal rotation as a function of radius at 75° latitude for an average over six years of HMI. Solid lines show the full-disk analysis and its error; errors for the other analysis were similar.

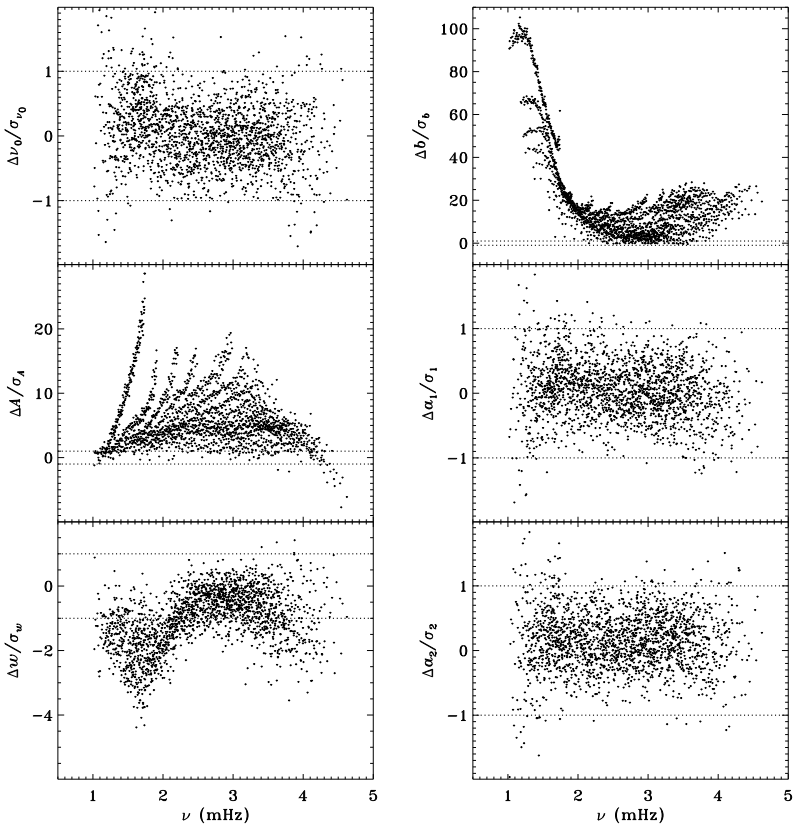

Figure 15. Difference between HMI and MDI full-disk fits for the 2010 dynamics run. Each panel is scaled differently; ~~dotted~~ **horizontal** lines show the $\pm 1\sigma$ levels. The sense of subtraction is HMI minus MDI.

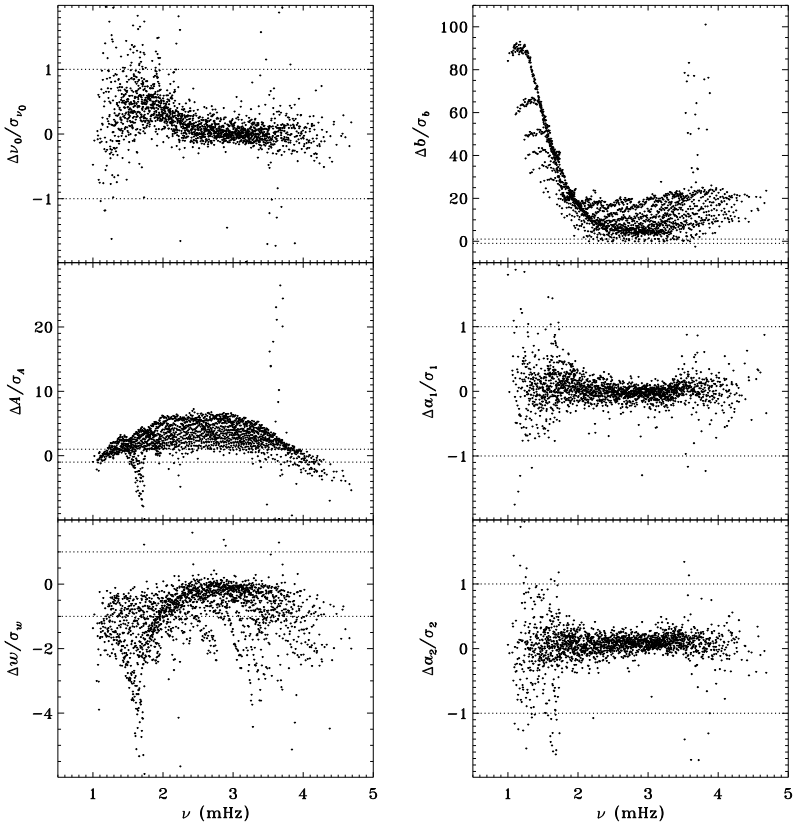

Figure 16. Difference between fits to the HMI vw_V proxy and MDI vw_V data for the first 72 days of HMI. Panels are scaled as in Figure 15 **for ease of comparison**, with ~~dotted~~ **horizontal** lines showing the $\pm 1\sigma$ levels. The sense of subtraction is HMI minus MDI.

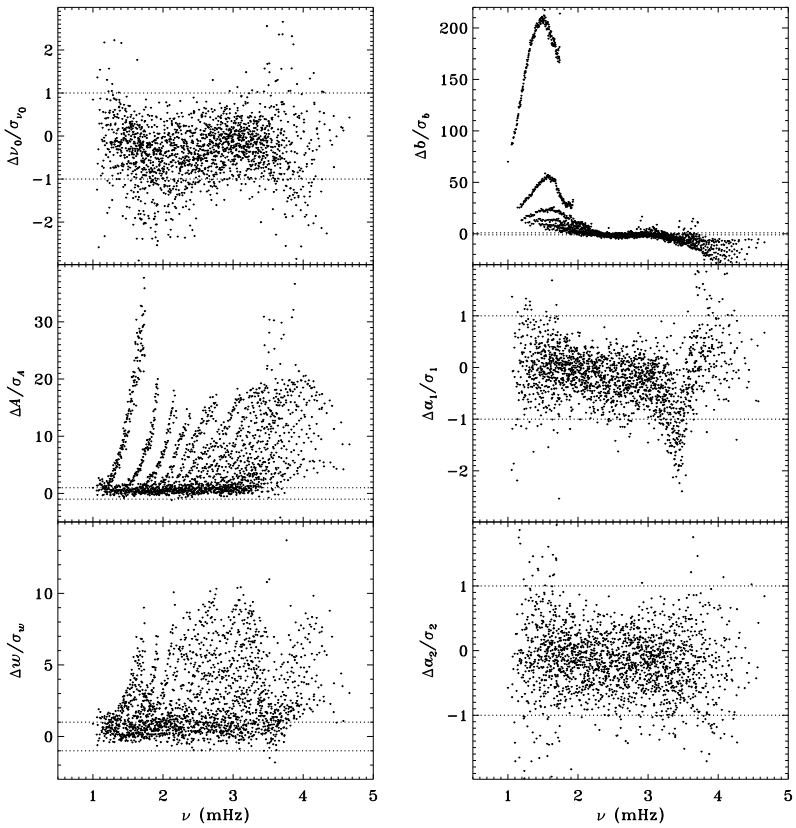

Figure 17. Difference between HMI full disk and vw_V proxy analyses for the first 72 days of HMI. Each panel is scaled differently; ~~dotted~~ **horizontal** lines show the $\pm 1\sigma$ levels. The sense of subtraction is full-disk minus vw_V proxy.

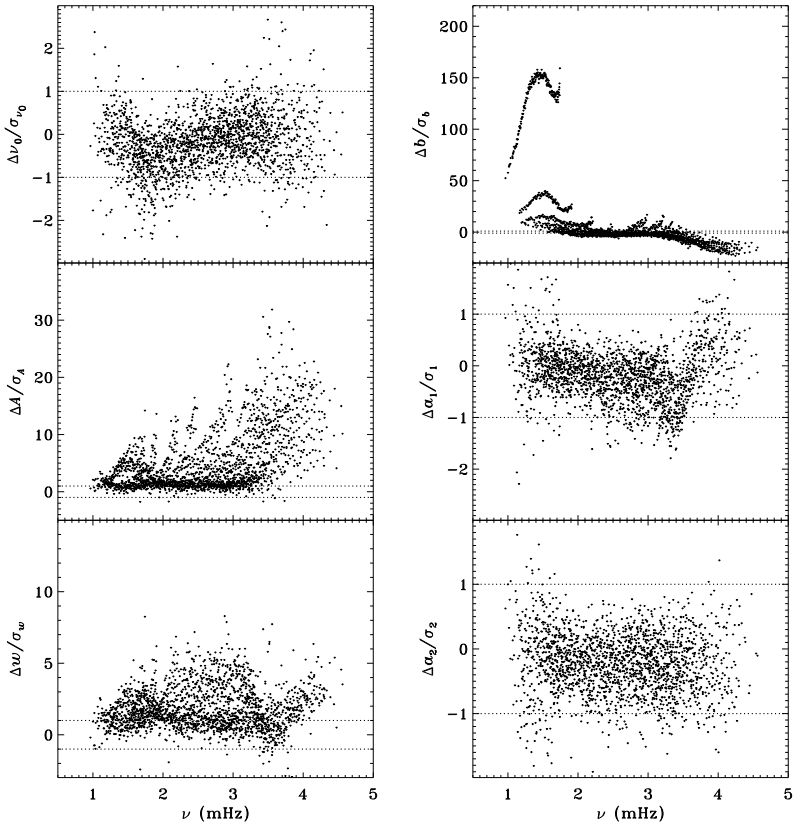

Figure 18. Difference between the MDI fd_ap90 and vw_ap83 analyses for the 2010 dynamics run. Panels are scaled as in Figure 17 **for ease of comparison**, with ~~dotted~~ **horizontal** lines showing the $\pm 1\sigma$ levels. The sense of subtraction is fd_ap90 minus vw_ap83.

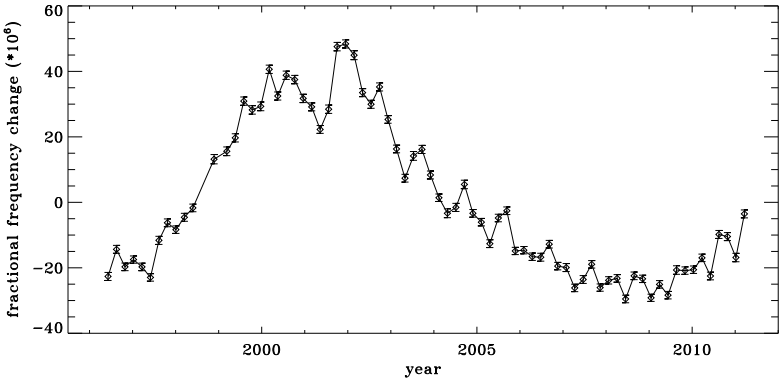

Figure 19. Fractional change in f-mode frequency for the entire MDI mission.

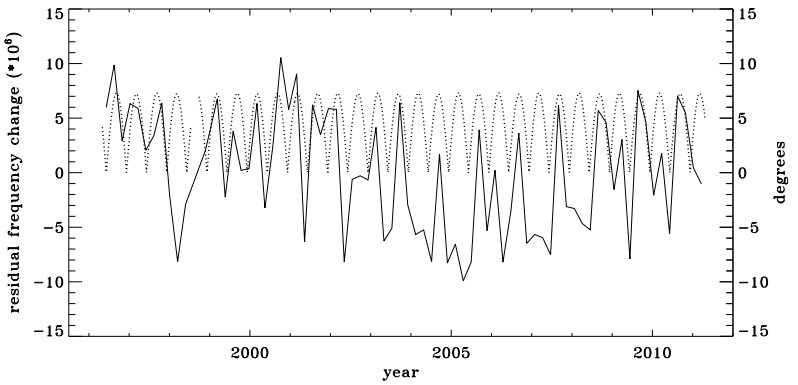

Figure 20. Fractional change in f-mode frequency for MDI with solar-cycle dependence removed. Overplotted is the absolute value of B_0.

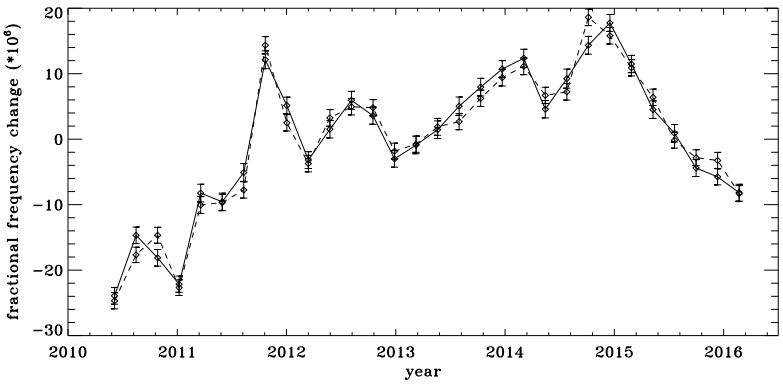

Figure 21. Fractional change in f-mode frequency for the first six years of HMI. Solid line shows the vw_V proxy, dashed line shows full-disk data.

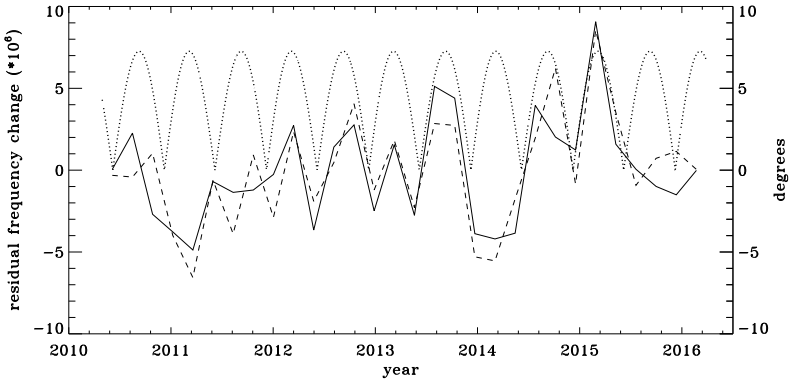

Figure 22. Fractional change in f-mode frequency for HMI with solar-cycle dependence removed. Solid line shows the vw_V proxy, dashed line shows full-disk data. Overplotted is the absolute value of B_0.

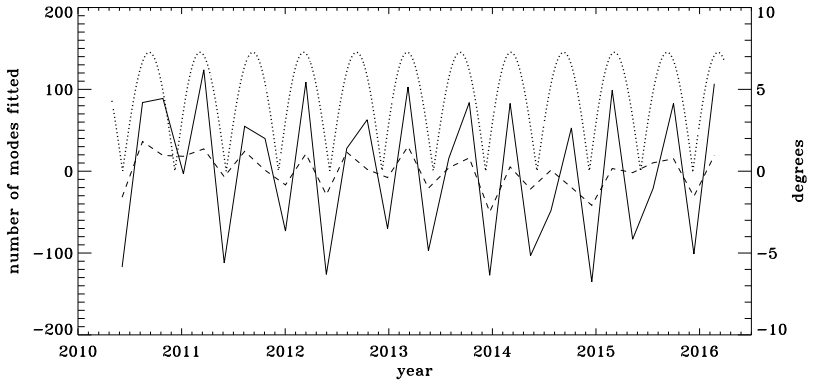

Figure 23. Number of modes fitted as a function of time for the HMI full-disk (dashed line) and the vw_V proxy (solid line) relative to their means (total number fitted shown in Figure 8). Overplotted is the absolute value of B_0.

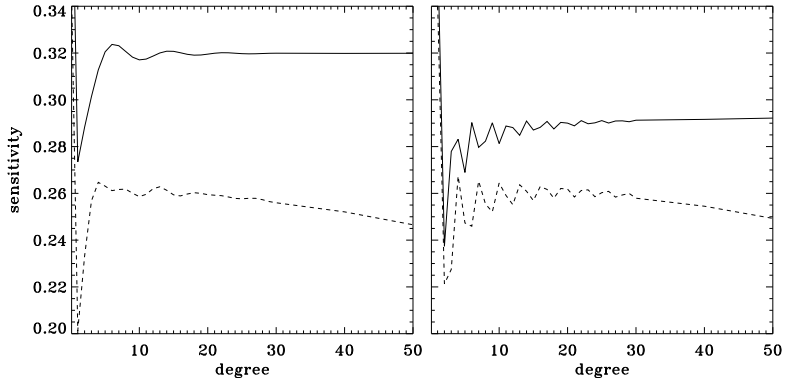

Figure 24. Sensitivity to target mode; left panel shows $m = 0$, right panel shows $m = \ell$. Solid lines show original leakage matrix, dashed lines show leaks for high $|B_0|$ ($= 6.35°$).

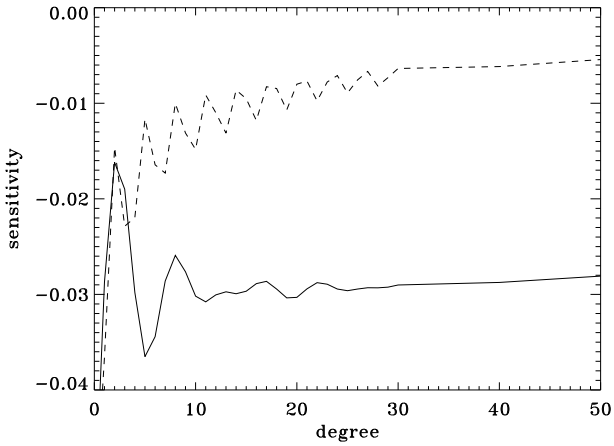

Figure 25. Leaks for $\Delta\ell = 1, \Delta m = 0$ and high $|B_0|$ ($= 6.35°$). Solid line shows $m = 0$, dashed line shows $m = \ell$. Original leaks are identically zero.

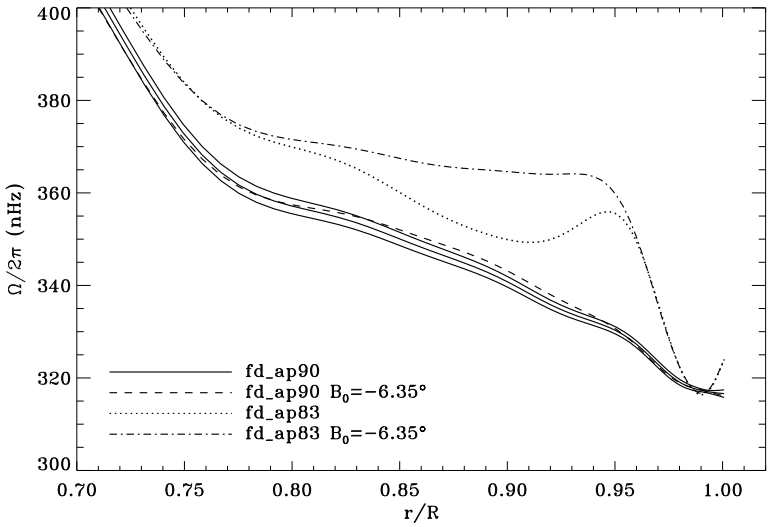

Figure 26. Effect of leakage matrix on inversions. Shown is internal rotation as a function of radius at 75° latitude for four analyses applied to the 1998 dynamics run. Two of the curves were shown in Figure 7. Solid lines show the fd_ap90 analysis and its error; errors for the other analyses were similar. For these inversions the full modesets were used, rather than common modesets.

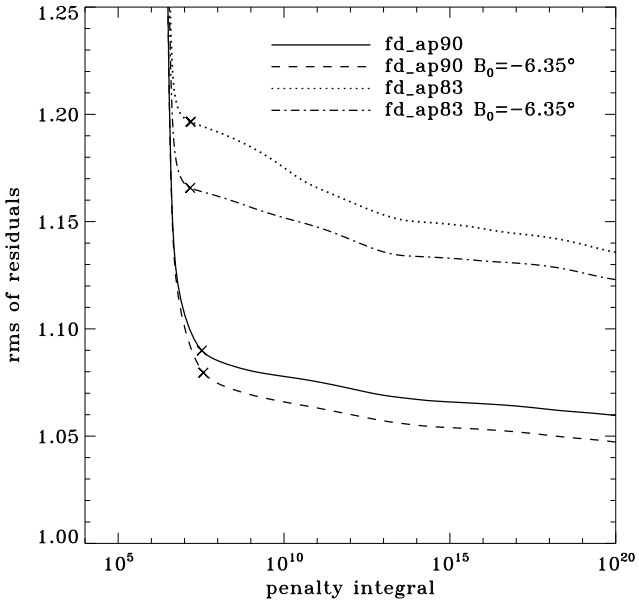

Figure 27. Effect of leakage matrix on residuals. Shown are tradeoff curves for four analyses applied to the 1998 dynamics run. Symbols indicate a tradeoff parameter of $\mu = 10^{-6}$. For these inversions the full modesets were used, rather than common modesets.

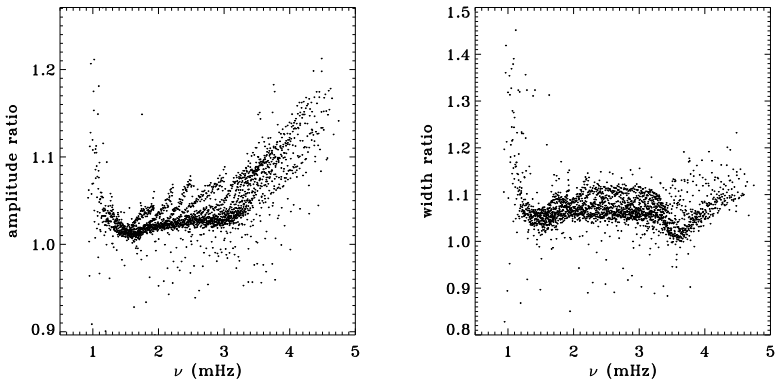

Figure 28. Ratios of amplitude and width from the fd_ap90 analysis to those from the fd_ap83 analysis for an average over all dynamics runs. For the width, 17 points have been excluded from the range shown.

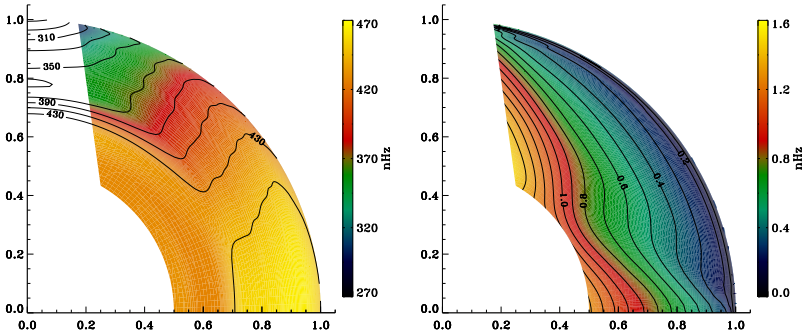

Figure 29. Internal rotation (left) and the corresponding errors (right) derived from the MDI full-disk analysis averaged over all dynamics runs. We have erased color from the regions where estimates of rotation are deemed unreliable; contours are retained on the left for ease of labeling.

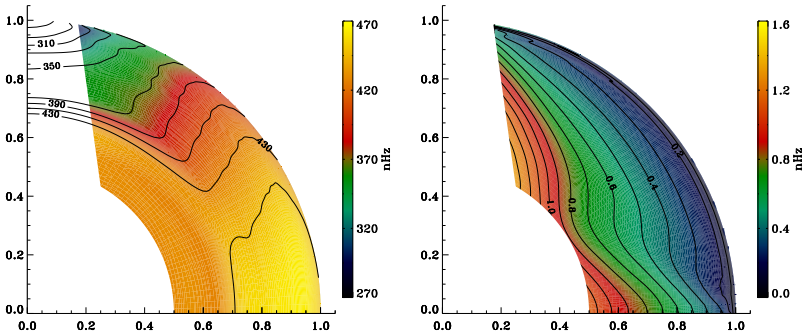

Figure 30. Internal rotation (left) and the corresponding errors (right) derived from an average over the first six years of the HMI 72-day analysis. We have erased color from the regions where estimates of rotation are deemed unreliable; contours are retained on the left for ease of labeling.